ACS APPLIED MATERIALS & INTERFACES

Nanostructure-Preserved Hematite Thin Film for Efficient Solar Water Splitting

Jae Young Kim,[†] Duck Hyun Youn,[†] Ju Hun Kim,[‡] Hyun Gyu Kim,[§] and Jae Sung Lee*,[†]

[†]Division of Energy and Chemical Engineering, Ulsan National Institute of Science and Technology (UNIST), 50 UNIST-gil, Ulsan 689-798, Republic of Korea

[‡]Department of Chemical Engineering, Pohang University of Science and Technology (POSTECH), 77 Cheongam-ro, Pohang 790-784, Republic of Korea

[§]Busan Center, Korea Basic Science Institute, Busan 609-735, Korea

Supporting Information

ABSTRACT: High-temperature annealing above 700 °C improves the activity of photoelectrochemical water oxidation by hematite photoanodes by increasing its crystallinity. Yet, it brings severe agglomeration of nanostructured hematite thin films and deteriorates electrical conductivity of the transparent conducting oxide (TCO) substrate. We report here that the nanostructure of the hematite and the conductivity of TCO could be preserved, while the high crystallinity is attained, by hybrid microwave annealing (HMA) utilizing a graphite susceptor for efficient microwave absorption. Thus, the hematite thin-film photoanodes treated by HMA record 2 times higher water oxidation photocurrents compared to a conventional thermal-annealed photoanode. The enhanced performance can be attributed to the synergistic effect of a smaller feature size of nanostructure-preserved hematite and a good electrical conductivity of TCO. The method could be generally applied to the fabrication of efficient photoelectrodes with small feature sizes and high crystallinity, which have been mutually conflicting requirements with conventional thermal annealing processes.

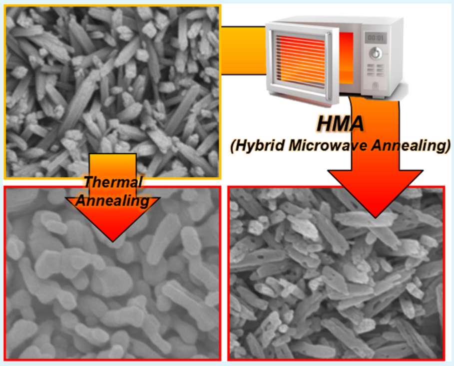

KEYWORDS: *nanostructures, crystallinity, solar water splitting, hematite, hybrid microwave annealing*

1. INTRODUCTION

Photoelectrochemical (PEC) solar water splitting is a promising route to produce hydrogen in a sustainable and eco-friendly manner.[1−4] Under illumination, photoexcited electron−hole pairs are generated in thin-film photoelectrodes, and they reduce and oxidize water, respectively, to evolve hydrogen and oxygen from the following reactions in case the anode is the light absorber:

$$\text{At anode: } 2H_2O(l) + h\nu \rightarrow O_2(g) + 4H^+ + 4e^- \tag{1}$$

$$\text{At cathode: } 2H^+ + 2e^- \rightarrow H_2(g) \tag{2}$$

Among many semiconductor photocatalysts, hematite (α-Fe_2O_3) has become one of the most popular photoanode materials past few years and achieved rapid progress to yield anodic photocurrents corresponding to solar-to-hydrogen conversion efficiency of as high as ca. 5%.[5−8] These high efficiency hematite photoanodes are obtained through many modifications to improve the poor electric property of hematite such as doping,[8−13] nanostructuring,[14,15] thermal annealing, and introducing an oxygen-evolving cocatalyst.[16−18] In particular, introduction of high-temperature annealing (>700 °C) is probably one of the most significant events responsible for the advent of many high-efficiency hematite thin films.[7] The high-temperature annealing is also known to bring unintentional doping due to diffusion of Sn from the FTO layer to the Fe_2O_3 bulk.[7] It has made hematite thin films routinely produce solar water oxidation photocurrents at mAcm^{-2} scale by forming highly crystalline hematite thin films with reduced defects and improved electrical conductivity.[8,19]

In spite of desirable effects of the high-temperature annealing, it also has a few drawbacks. First, the electrical conductivity of transparent conducting oxide (TCO) employed as the substrate of photoelectrodes deteriorates with conventional thermal annealing (CTA) above ~550 °C.[20,21] In this case, "conventional thermal annealing" refers to any kind of annealing procedure using a "conventional thermal furnace". Second, hematite thin film agglomerates, and its original nanostructure formed at low temperatures is severely damaged. The growth of the feature size is a critical issue especially for photocatalytic materials like hematite, which has an extremely short hole diffusion length of 2−4 nm.[22,23] Due to the short hole diffusion length, it is hard for the photoexcited holes formed in the bulk to diffuse to the electrode|electrolyte interface before charge recombination occurs in the materials with large feature sizes.

Received: April 20, 2015
Accepted: June 5, 2015
Published: June 5, 2015

DOI: 10.1021/acsami.5b03409
ACS Appl. Mater. Interfaces 2015, 7, 14123−14129

In fact, this represents a long-standing dilemma in preparing efficient optoelectronic materials. Most desired is high crystallinity without defects and small feature sizes, yet CTA yields high crystallinity but large feature sizes by sintering, thereby forcing us to compromise between crystallinity and size. There have been only a few reports that specifically address this challenge. An example is to use a structure confinement scaffold.[24] Thus, SiO_2 scaffold encapsulates the original Fe_2O_3 structure to help it endure high-temperature annealing without serious growth of the feature size. Yet, this method cannot avoid deteriorated electrical conductivity of TCO substrate, and the scaffold has to be removed later, making the overall process complicated.

As our approach to meet this challenge, here we report an ingenious method to prepare semiconductor electrodes of high crystallinity, still maintaining small feature sizes. Thus, highly crystalline nanostructure-preserved hematite thin films were prepared by the hybrid microwave annealing (HMA) technique. The electrical conductivity of F-doped SnO_2 (FTO) substrate was also not much damaged either. Furthermore, we believe HMA could be generally applied to the fabrication of efficient photoelectrodes of other semiconductors due to its simple and facile process, as we recently demonstrated for $ZnFe_2O_4$,[25] CuO,[26] and MoS_2.[27]

The HMA combines conventional microwave heating with an additional heating from an effective microwave absorber called a susceptor.[25] Briefly, the temperature of a susceptor (graphite) increases immediately upon microwave irradiation, and the susceptor transfers the heat to the sample by the conventional heating mechanisms. Then, the heated sample could absorb the microwave effectively due to the changed dielectric properties and attenuation distance at the elevated temperature. Due to the efficiency of the HMA process, annealing of hematite electrode is completed in a few minutes, and thus, crystal growth and deterioration of FTO are minimized. Furthermore, HMA could be an innovative technique with several other advantages in energy saving and process safety. Optimum annealing time for HMA (5 min) is shorter than that for CTA (20 min), and the difference becomes more significant when considering the time required for ramping and cooling processes for CTA. Thus, energy required for annealing of hematite thin films is proportionally smaller for HMA compared to CTA. HMA is also a relatively safer annealing process without the need to take samples in/out of the preheated furnace.

2. EXPERIMENTAL SECTION

2.1. Electrode Fabrication. The hematite photoanodes were prepared via a simple solution-based method and high-temperature annealing at 800 °C.[28,29] A starting material (β-FeOOH) is grown on substrate (F:SnO_2-coated glass, FTO, purchased from Pilkington Inc., model: TEC8) at 100 °C in aqueous solution containing Fe precursor (0.15 M $FeCl_3 \cdot H_2O$) and 1 M $NaNO_3$. The reactor containing the solution and FTO glass pieces was kept in an oven for 6 h, and the resultant substrate coated with yellow thin film was washed with excess amount of distilled water. After drying at ambient temperature and pressure overnight, the thin film was annealed at 800 °C for 20 min using a conventional thermal furnace. To minimize damage, the thin film was put into the preheated furnace and taken from the furnace right after 20 min. For hybrid microwave annealing, a Pyrex beaker containing 8 g of graphite powder (susceptor) was prepared, and the yellow thin film was slightly buried on the flat surface of the graphite to expose only the top surface of the thin film (Scheme S1 of Supporting Information, SI). The beaker was put inside a household microwave oven of 2.45 GHz and 800W, and the annealing was performed for 2−15 min.

2.2. Electrochemical Measurements. The photoanode was put in a three-electrode cell as a working electrode to observe its solar water oxidation response. A platinum mesh electrode and Ag/AgCl electrode were also employed in the cell as a counter electrode and reference electrode. One molar sodium hydroxide was used for basic (pH 13.6) electrolyte. Photocurrent−potential curves and electrochemical impedance spectra were recorded under simulated solar light generated by a solar simulator (91170, Oriel) with an air mass 1.5 G filter. Light intensity of the solar simulator was calibrated to 1 sun (100 mW/cm^2) using a reference cell certified by the National Renewable Energy Laboratories, U.S. All electrochemical measurements were performed using a potentiostat (IviumStat, Ivium Technologies). Electrochemical impedance spectra (EIS) were recorded at DC potential 1.23 V vs RHE and an AC potential frequency range of 100000−0.1 Hz with an amplitude of 10 mV. A software (ZView, Scribner Associates) was used for fitting the experimental EIS data to the equivalent circuit model.

2.3. Catalyst Characterization. In order to characterize the hematite thin films, X-ray diffraction analysis (PW3040/60 X'pert PRO, PANalytical with Cu Kα (λ = 1.54056 Å) radiation), HR-TEM (JEM-2200FS, JEOL with Cs-corrector in the National Institute for Nanomaterials Technology, Republic of Korea), HR-SEM (JSM-7401F, JEOL), XPS (K-Alpha, Thermo Fisher), UV−vis (UV-3600, SHIMADZU) were used. Detailed conditions for catalyst characterization are included in Table S1 in SI. The powder was prepared by grinding the hematite thin-film surface with a sand paper for HR-TEM. The powders were dispersed with a suitable amount in ethanol (for HR-TEM).

3. RESULTS AND DISCUSSION

3.1. Crystal Structure and Morphology of Hematite Depending on Annealing Methods. The precursor to hematite used in the present study was prepared by a modified version of the template-less thin-film processing technique reported earlier.[28,29] Thus, a highly anisotropic β-FeOOH akaganeite film on FTO-coated glass from an aqueous $FeCl_3 \cdot 6H_2O$ solution was synthesized in such a condition that the thermodynamic stabilization of the oxyhydroxide structure could be secured. This β-FeOOH nanostructure on FTO was then converted to α-Fe_2O_3 by different annealing methods (i.e., CTA and HMA).

For HMA, a Pyrex beaker containing 8 g of graphite powder was used as a susceptor, and a FeOOH thin film was slightly buried in the graphite powder so that only the surface of the thin film is exposed to the air (Scheme S1). The HMA treatment was performed with a household microwave oven of 2.45 GHz and 800W for 2−15 min. For CTA, the FeOOH thin film was annealed at 800 °C for 20 min in a muffle furnace. This high-temperature annealing has been known to produce hematite thin films of high crystallinity with reduced defects and high solar water oxidation activity.[7,19] As shown in the X-ray diffraction (XRD) patterns of Figure S1 of SI, hematite shows a dominant (110) peak at 2θ = 35.8°, indicating preferential orientation of hematite crystals in this direction.[30−32] The peak gets stronger for longer annealing times in both HMA and CTA. However, the effect is saturated after 5 min of HMA and 20 min of CTA. The crystallinity represented by the XRD peak was very similar for hematite electrodes treated by 5 min of HMA and 20 min of CTA. The HRTEM images in Figure 1 also show that the nanorods are single crystalline with well-defined lattice fringes denoting preferential [110] orientation. The insets show (110) XRD peaks for each thin film of the similar intensity. Hence, both CTA and HMA of β-FeOOH produced α-Fe_2O_3 of the same high crystallinity.

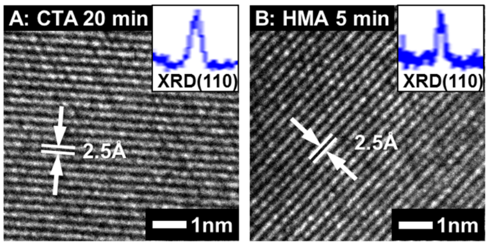

Figure 1. High-resolution TEM images of the hematite thin film annealed by two different conditions: (A) 20 min of a conventional thermal annealing (CTA); (B) 5 min of hybrid microwave annealing (HMA). The insets show (110) X-ray diffraction peak for each thin film representing similar high crystallinity with well-defined lattice fringes denoting preferential [110] orientation in both films.

Unlike the same crystal structure, the hematite thin films have very different morphologies depending upon annealing methods as shown in the SEM images of Figure 2. First, β-FeOOH akaganeite on FTO has the morphology of nanorods with a diameter of ~30 nm (Figure 2A). This β-FeOOH nanostructure was then converted to α-Fe_2O_3 by annealing treatment. After CTA at 800 °C for 20 min, nanorods turned to wormlike particles of ~70 nm (Figure 2B). On the other hand, it maintained its nanorod morphology with only slightly increased diameter of ~40 nm after HMA for 5 min (Figure 2C). Cross-sectional SEM images also demonstrate the nanorod-type morphology for the HMA hematite thin film compared to the agglomerated wormlike morphology for the CTA hematite film. Thus, the HMA treatment preserves the initial nanorod morphology while greatly improving crystallinity of hematite. In addition, the sheet resistance of FTO substrate was determined by four-probe measurements, as summarized in Table S2. The resistance remained unaltered during HMA for 15 min, whereas it gradually and continuously increased with time during CTA. As evidenced by the previous attempts to improve conducting property of substrate by introduction of good conducting scaffold[33] or ultrathin metal layer,[34] change on substrate conductivity is a significant parameter which affects the final water oxidation performance. Table S2 of SI also shows the surface temperature of the sample determined by infrared thermometer laser gun. After 5 min of HMA, the temperature was determined to be 650 °C. The effectiveness of HMA should be noted here that the annealing at even lower temperature and shorter time gives as high the crystallinity as obtained by CTA at higher temperature (800 °C) and longer time (20 min). In any case, this relatively low temperature and the short processing time of HMA seem responsible for the preservation of the nanostructure and maintenance of the electric conductivity of FTO substrate.

To observe reported Sn diffusion from FTO layer to the Fe_2O_3 bulk[7,35] during CTA and HMA, XPS spectra of Sn were obtained (Figure S2). In Figure S2A, Sn diffusion is clearly observed for both HMA and CTA hematite. The intensity of Sn XPS peak was slightly smaller for HMA hematite reflecting its relatively lower temperature and shorter annealing time. Meanwhile, carbon was detected for both CTA and HMA hematite as C 1s spectra indicated (Figure S2D). However, the presence of the same C 1s spectrum of the similar intensity for the unannealed thin film (β-FeOOH) indicates that that carbon has mainly originated from air, not from the graphite susceptor during the HMA process.

3.2. Solar Water Splitting.

The solar water splitting performance of the hematite thin-film photoanodes was investigated under simulated 1 sun (100 mW, AM 1.5) illumination. As shown in current (J)−potential (V) curves of Figure 3, the optimum annealing times that gave the maximum photocurrent generation were 5 min for HMA and 20 min for CTA. For the optimized electrodes, water oxidation photocurrents were 1.58 mAcm^{-2} for HMA and 0.86 mAcm^{-2} for CTA at 1.23 V_{RHE}. Thus, the water oxidation photocurrent was ~2 times higher for the case of HMA. In addition, HMA shifted onset potential of photocurrent to cathodic direction by ~0.2 V (Figure 3C).

Considering the confirmed merits of HMA and the fact that both electrodes have similar crystallinity, this improvement can be mainly attributed to the smaller feature size of hematite thin film and the preserved electrical conductivity of the FTO substrate. The former effect can facilitate hole transfer at the electrode||electrolyte interface, whereas the latter can facilitate electron transfer at electrode|substrate interface. That is, charge separation could be accelerated by the synergistic effect of the small feature size of the electrode and the good electrical conductivity of the FTO substrate. Because unintentional Sn

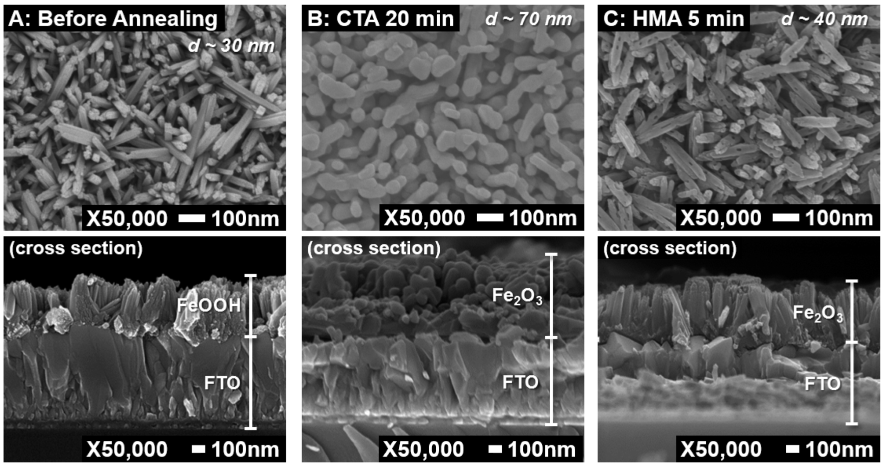

Figure 2. High-resolution SEM images showing surface morphology of the thin films. (A) Iron oxyhydroxide (β-FeOOH) thin film before annealing; (B) Hematite thin film after 20 min of conventional thermal annealing (CTA); (C) Hematite thin film after 5 min of hybrid microwave annealing (HMA). The second row shows cross-sectional view for each film.

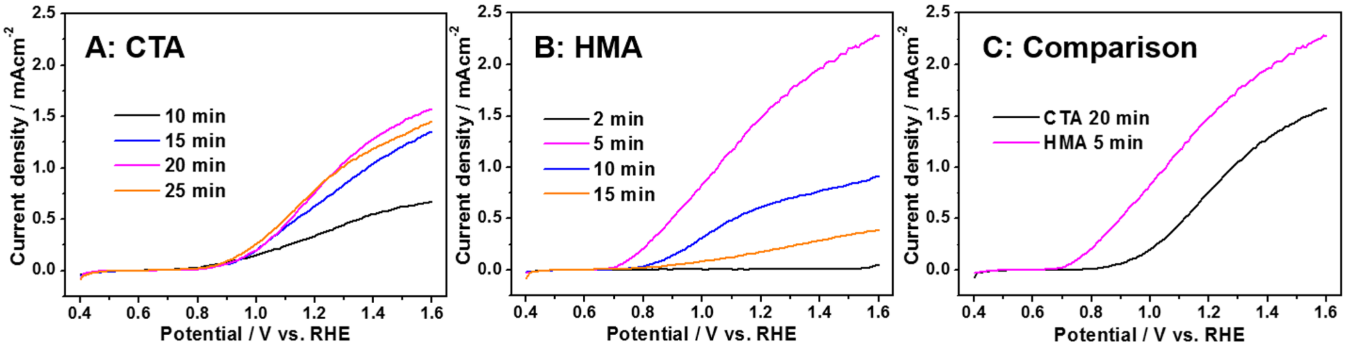

Figure 3. Water oxidation photocurrent (J)−potential (V) curves recorded with the hematite thin-film photoanodes treated by CTA (A) and HMA (B). The optimum annealing time was found to be 20 and 5 min, respectively. C: Additional J−V curve for comparison of the optimum water oxidation photocurrents generated from CTA and HMA.

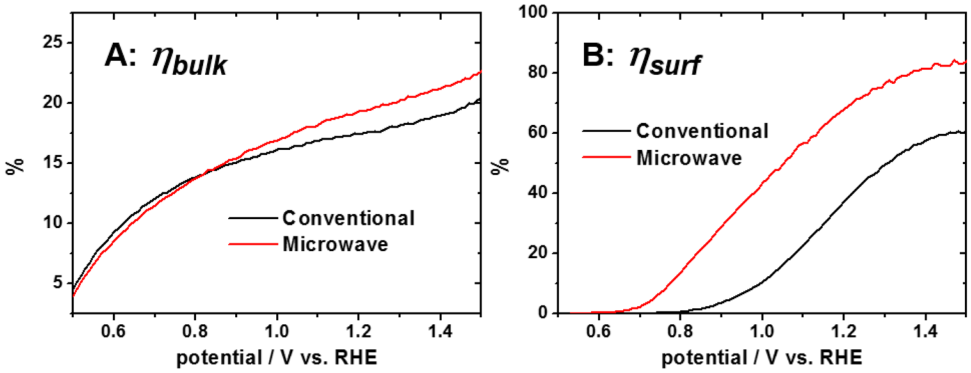

Figure 4. Bulk (A) and surface (B) charge separation efficiency vs potential calculated from the eqs 3 and 4, and photocurrents measured with electrolytes containing 0.5 M H_2O_2.

doping by its diffusion from FTO substrate is observed for both HMA and CTA electrodes, its effect does not contribute to the difference in the their PEC performance. To the best of our knowledge, microwave-assisted annealing of hematite was reported only once.[36] However, because of the improper choice of susceptor and operating conditions, the annealing temperature remained below 300 °C, and their best photocurrent obtained at 1.23 V_{RHE} (107 μA/cm^2) was lower than our case (1.58 mAcm^{-2}) by a factor of ∼15. It appears that the optimum annealing time for HMA (5 min) is determined by the abrupt agglomeration of hematite thin films at longer annealing times (Figure S3). Thus, the original nanostructure of hematite thin films dramatically changed to wormlike particles of large feature sizes, although the electrical conductivity of substrate is maintained up to 20 min of HMA (Table S2). It is noted that HMA is a highly sensitive annealing technique with a narrow optimum time window (Figure S4). With the optimum annealing time, HMA hematite has crystallinity as good as that of CTA hematite, whereas its nanostructure and the conductivity of the FTO substrate are preserved.

3.3. Photoelectrochemical Investigations. In order to understand the origin of favorable effects of HMA over CTA, the photoelectrochemical properties of photoanodes were further investigated. Both HMA and CTA hematite thin films have similar optical properties, including band gap energy (∼2.1 eV) and light-harvesting efficiency (Figure S5). The small difference in light-harvesting efficiency (90−86% for HMA and 94−90% for CTA at $\lambda < 550$ nm) is not significant. It is also noteworthy that both films show steep absorption edges all the way to ∼600 nm. Because hematite has an indirect band gap, it usually shows a small absorbance near the band gap energy.[5] The high crystallinity of both samples obtained by the high-temperature annealing may be responsible for the high absorbance at long wavelengths.

Next, the charge separation efficiencies were estimated on the surface and the bulk of hematite thin-film photoanodes (Figure 4). We calculated these charge separation efficiencies by comparing J−V curves in Figure S6 for photooxidation of water (J^{H_2O}) and hole scavenger (in 0.5 M H_2O_2, $J^{H_2O_2}$).[37]

$$J^{H_2O} = J_{ab} \times \eta_{bulk} \times \eta_{surf} \tag{3}$$

Because of the rapid kinetics of H_2O_2 photooxidation, its surface charge separation efficiency η_{surf} is practically 100%, hence:

$$J^{H_2O_2} = J_{ab} \times \eta_{bulk} \tag{4}$$

The η_{surf} for water oxidation is obtained simply from the ratio of $J^{H_2O}/J^{H_2O_2}$. Absorbed incoming light intensity (J_{ab}) was determined to be 11.3 mAcm^{-2} for HMA and 11.7 mAcm^{-2} for CTA based on eq 5. These values are also unusually high close to the theoretical value of 12.5 mAcm^{-2} and reflect the high absorbance as discussed above.

$$J_{ab} = \int_{300}^{600} \frac{1}{1240} \lambda \cdot E(\lambda) \cdot \eta_{LH}(\lambda) d\lambda \tag{5}$$

Here, $E(\lambda)$ represents solar irradiance and we used ASTM G-173-03 as a reference for solar irradiance. $\eta_{LH}(\lambda)$ represents light-harvesting efficiency and can be extracted from light absorbance, as shown in Figure S5. Then η_{bulk} values could be calculated. As in Figure 4A, both HMA and CTA hematite films

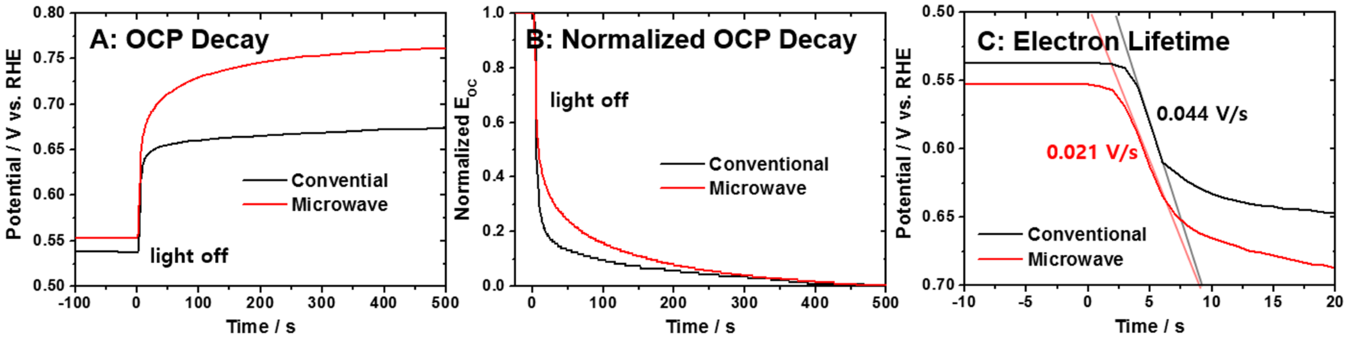

Figure 5. (A) Open circuit potential (OCP) decay diagram recorded by turning off the light at steady state under illumination. (B) Normalized OCP decay diagram; (C) Enlarged OCP decay diagram of A.

show similar values of bulk charge separation efficiency (η_{bulk}) over the most of the potential range. On the other hand, surface charge separation efficiency (Figure 4B) of HMA hematite photoanodes consistently exceeds that of CTA photoanodes by 20−30% over the whole potential range. Their almost the same η_{bulk} values seem to originate from their similar crystallinity and [110] preferential orientation, as confirmed by XRD and TEM, which is known as the best direction for charge transfer.[5,30] Meanwhile, η_{surf} can be affected by the facilitated hole transfer at electrode||electrolyte interface due to the smaller feature size of HMA hematite morphology. That is, the possibility that photoexcited holes survive the recombination increases in smaller feature sized materials because travel the length of the holes to electrode||electrolyte interface becomes shorter. Another possibility for the higher η_{surf} is that the enlarged electrode surface area of HMA hematite helps hole consumption by water oxidation reaction at electrode||electrolyte interface (Figure 2B,C).

The dynamic nature of the charge carriers could be monitored by measuring open circuit potential (OCP) decay and electron lifetime in electrode calculated from the OCP decay results as shown in Figure 5.[38−41] The OCP decay was recorded by turning off the light after achieving steady state under illumination. Photovoltage, V_{ph}, was determined as 0.14 and 0.21 V for CTA and HMA hematite photoanodes, respectively (Figure 5A). It shows the same tendency as the onset potential shift of water oxidation photocurrent (Figure 3C).[39,40] In addition, it could be an indication of a smaller amount of surface state on HMA hematite surface compared to CTA surface.

The OCP decay rate (dV_{OC}/dt) is slower for HMA hematite photoanodes, which is more clearly observed in normalized OCP decay diagram (Figure 5B).[40] Electron lifetime, τ_n, could be extracted from the linear part of the enlarged OCP decay diagram (Figure 5C) on the basis of the following equation.[41]

$$\tau_{\mathrm{n}} = -\frac{k_{\mathrm{B}}T}{e}\left(\frac{dV_{\mathrm{OC}}}{dt}\right) \qquad (6)$$

The electron lifetimes were determined to be 0.58 and 1.22 s, respectively, for CTA and HMA hematite photoanodes. Longer electron lifetimes make electrons possible to travel longer distances without charge recombination. Therefore, electron transfer is expected to be faster in HMA hematite photoanodes.

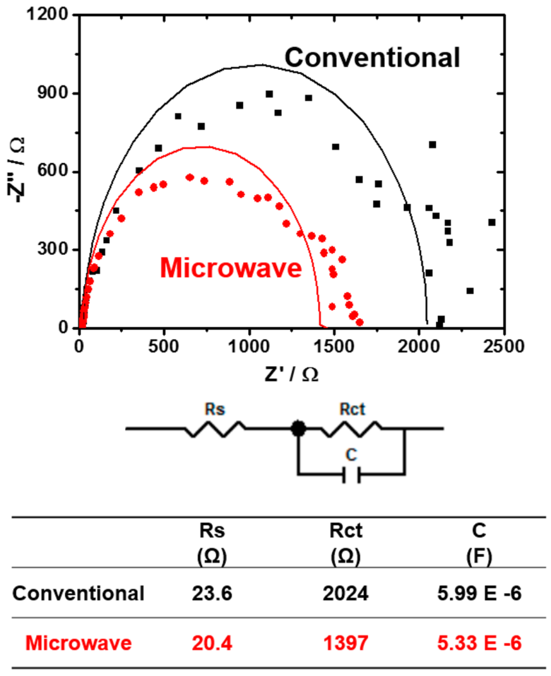

	Rs (Ω)	Rct (Ω)	C (F)
Conventional	23.6	2024	5.99 E -6
Microwave	20.4	1397	5.33 E -6

Figure 6. Electrochemical impedance spectra (Nyquist plots, top), the equivalent circuit model (middle), and the fitting results (bottom) for the hematite thin films annealed by CTA and HMA.

The charge transfer characteristic in hematite electrodes alluded to above was studied by electrochemical impedance spectroscopy (EIS) in Figure 6. In the Nyquist plots, the experimental data were fitted to a Randle circuit with three elements: R_{ct} (charge transfer resistance at electrode||electrolyte interface), C (Helmholtz layer capacitance), R_{s} (all remaining resistances involved in the photoanode).[42,43] Among them, R_{ct} was reduced by 30% for HMA hematite photoanodes due to the enhanced solar water oxidation rate on the surface of the photoanodes. According to the Mott−Schottky plots in Figure S7, CTA and HMA hematite thin films have a similar donor density of ∼10^{17} cm^{-3} but different flat band potentials; 0.53 V_{RHE} for CTA and 0.41 V_{RHE} for HMA hematite thin films. Hence, the results show that HMA does not affect donor density of hematite thin films but shifts flat band potential to cathodic values relative to CTA hematite, which is consistent with the cathodic shift of onset potential of water oxidation photocurrent (V_{onset}, Figure 3C) and increased photovoltage (V_{ph}, Figure 5A).[38,39,44] Thus, the shift of onset potential of solar water oxidation (∼200 mV) is well explained by the increased photovoltage (∼70 mV) and the shift of flat band potential (∼120 mV). Onset potential of solar water oxidation can be affected by surface states of semiconductor thin films.[38,39] Thus, HMA hematite thin films might have less surface states so that photovoltage becomes larger and flat band potential shifts to the cathodic direction. These improved surface properties of HMA result in the high surface charge separation efficiency and enhanced water oxidation kinetics (Figure 4B).

4. CONCLUSION

Fabrication of high crystalline and nanostructured semiconductors of small feature sizes has been a long-standing thrust to prepare efficient optoelectronic materials. Here we propose that HMA could be such a general method by reporting nanostructure-preserved hematite thin films of high crystallinity that show an excellent activity of solar water splitting far exceeding the material prepared by CTA. HMA hematite thin films had smaller feature size in morphology and less damaged electrical conductivity compared to CTA hematite thin films by preventing agglomeration of the original nanostructure and severe damage on substrate. As a result, charge separation could be accelerated by the synergistic effect of the small feature size of hematite (hole transfer at electrode||electrolyte interface) and the good electrical conductivity of substrate (electron transfer at electrode|subsrate interface) resulting in efficient solar water splitting performance (2 times higher than that of CTA hematite photoanodes). In addition, the current annealing method is a simple and easy method compared to the complicated structure confinement scaffold method discussed earlier.

■ ASSOCIATED CONTENT

Ⓢ Supporting Information

XRD, XPS, four-probe measurement, UV−vis spectroscopy, and Mott−Schottky analysis results. The Supporting Information is available free of charge on the ACS Publications website at DOI: 10.1021/acsami.5b03409.

■ AUTHOR INFORMATION

Corresponding Author

*E-mail: jlee1234@unist.ac.kr.

Author Contributions

The manuscript was written through contributions of all authors. All authors have given approval to the final version of the manuscript.

Notes

The authors declare no competing financial interest.

■ ACKNOWLEDGMENTS

This work was supported by Brain Korea Plus Program of Ministry of Education, Korean Center for Artificial Photosynthesis (NRF-2011-C1AAA0001-2011-0030278) funded by MISIP and Project No. 10050509 funded by MOTIE of Republic of Korea. It was also supported by Ulsan National Institute of Science and technology (UNIST).

■ ABBREVIATIONS

CTA, conventional thermal annealing
HMA, hybrid microwave annealing

■ REFERENCES

(1) Fujishima, A.; Honda, K. Electrochemical Photolysis of Water at a Semiconductor Electrode. *Nature* **1972**, *238*, 37−38.

(2) Walter, M. G.; Warren, E. L.; McKone, J. R.; Boettcher, S. W.; Mi, Q.; Santori, E. A.; Lewis, N. S. Solar Water Splitting Cells. *Chem. Rev.* **2010**, *110*, 6446−6473.

(3) Tachibana, Y.; Vayssieres, L.; Durrant, J. R. Artificial Photosynthesis for Solar Water-Splitting. *Nat. Photonics* **2012**, *6*, 511−518.

(4) Bard, A. J.; Fox, M. A. Artificial Photosynthesis: Solar Splitting of Water to Hydrogen and Oxygen. *Acc. Chem. Res.* **1995**, *28*, 141−145.

(5) Sivula, K.; Le Formal, F.; Grätzel, M. Solar Water Splitting: Progress Using Hematite (α-Fe_2O_3) Photoelecctrodes. *ChemSusChem* **2011**, *4*, 432−449.

(6) Ling, Y.; Wang, G.; Reddy, J.; Wang, C.; Zhang, J. Z.; Li, Y. The Influence of Oxygen Content on the Thermal Activation of Hematite Nanowires. *Angew. Chem., Int. Ed.* **2012**, *124*, 4150−4155.

(7) Sivula, K.; Zboril, R.; Le Formal, F.; Robert, R.; Weidenkaff, A.; Tucek, J.; Frydrich, J.; Grätzel, M. Photoelectrochemical Water Splitting with Mesoporous Hematite Prepared by a Solution-Based Colloidal Approach. *J. Am. Chem. Soc.* **2010**, *132*, 7436−7444.

(8) Kim, J. Y.; Magesh, G.; Youn, D. H.; Jang, J.-W.; Kubota, J.; Domen, K.; Lee, J. S. Single-Crystalline, Wormlike Hematite Photoanodes for Efficient Solar Water Splitting. *Sci. Rep.* **2013**, *3*, 2681.

(9) Hu, Y.-S.; Kleiman-Shwarsctein, A.; Forman, A. J.; Hazen, D.; Park, J.-N.; McFarland, E. W. Pt-doped α-Fe_2O_3Thin films Active for Photoelectrochemical Water Splitting. *Chem. Mater.* **2008**, *20*, 3803−3805.

(10) Cesar, I.; Kay, A.; Gonzalez Martinez, J. A.; Grätzel, M. Translucent Thin Film Fe_2O_3 Photoanodes for Efficient Water Splitting by Sunlight: Nanostructure-Directing Effect of Si-Doping. *J. Am. Chem. Soc.* **2006**, *128*, 4582−4583.

(11) Choi, J.; Park, H.; Hoffmann, M. R. Combinatorial Doping of TiO2 with Platinum (Pt), Chromium (Cr), Vanadium (V), and Nickel (Ni) to Achieve Enhanced Photocatalytic Activity with Visible Light Irradiation. *J. Mater. Res.* **2010**, *25*, 149−158.

(12) Jo, W. J.; Jang, J.-W.; Kong, K.-j.; Kang, H. J.; Kim, J. Y.; Jun, H.; Parmar, K. P. S.; Lee, J. S. Phosphate Doping into Monoclinic $BiVO_4$ for Enhanced Photoelectrochemical Water Oxidation Activity. *Angew. Chem., Int. Ed.* **2012**, *51*, 3147−3151.

(13) Mao, A.; Park, J.-G.; Han, G. Y.; Park, J. H. Controlled Growth of Vertically Oriented Hematite/Pt Composite Nanorod Arrays: Use for Photoelectrochemical Water Splitting. *Nanotechnology* **2011**, *22*, 175703.

(14) Kim, H. G.; Borse, P. H.; Jang, J. S.; Ahn, C. W.; Jeong, E. D.; Lee, J. S. Engineered Nanorod Perovskite Film Photocatalysts to Harvest Visible Light. *Adv. Mater.* **2011**, *23*, 2088−2092.

(15) Jun, H.; Im, B.; Kim, J. Y.; Im, Y.-O.; Jang, J.-W.; Kim, E. S.; Kim, J. Y.; Kang, H. J.; Hong, S. J.; Lee, J. S. Photoelectrochemical Water Splitting over Ordered Honeycomb Hematite Electrodes Stabilized by Alumina Shielding. *Energy Environ. Sci.* **2012**, *5*, 6375−6382.

(16) Kanan, M. W.; Surendranath, Y.; Nocera, D. G. Cobalt-Phosphate Oxygen-Evolving Compound. *Chem. Soc. Res.* **2009**, *38*, 109−114.

(17) Zhong, D. K.; Cornuz, M.; Sivula, K.; Grätzel, M.; Gamelin, D. R. Photo-Assisted Electrodeposition of Cobalt-Phosphate (Co-Pi) Catalyst on Hematite photoanodes for Solar Water Oxidation. *Energy Environ. Sci.* **2011**, *4*, 1759−1764.

(18) Kim, J. Y.; Jang, J.-W.; Youn, D. H.; Magesh, G.; Lee, J. S. A Stable and Efficient Hematite Photoanode in a Neutral Electrolyte for Solar Water Splitting: Towards Stability Engineering. *Adv. Energy Mater.* **2014**, *4*, 1400476.

(19) Ling, Y.; Wang, G.; Wheeler, D. A.; Zhang, J. Z.; Li, Y. Sn-Doped Hematite Nanostructures for Photoelectrochemical Water Splitting. *Nano Lett.* **2011**, *11*, 2119−2125.

(20) Kashiwa, Y.; Yoshida, Y.; Hayase, S. All-Metal-Electrode-Type Dye Sensitized Solar Cells (Transparent Conductive Oxide-Less Dye Sensitized Solar Cell) Consisting of Thick Porous Ti Electrode with Straight Pores. *Appl. Phys. Lett.* **2008**, *92*, 033308.

(21) Paulose, M.; Shankar, K.; Varghese, O. K.; Mor, G. K.; Grimes, C. A. Application of Highly-Ordered TiO2 Nanotube-Arrays in Heterojunction Dye-Sensitized Solar Cells. *J. Phys. D: Appl. Phys.* **2006**, *39*, 2498−2503.

(22) Kennedy, J. H.; Frese, K. W. Photooxidation of Water at α-Fe_2O_3 Electrodes. *J. Electrochem. Soc.* **1978**, *125*, 709−714.

(23) Tilley, S. D.; Cornuz, M.; Sivula, K.; Grätzel, M. Light-Induced Water Splitting with Hematite: Improved Nanostructure and Iridium Oxide Catalysis. *Angew. Chem., Int. Ed.* **2010**, *49*, 6405−6408.

(24) Brillet, J.; Grätzel, M.; Sivula, K. Decoupling Feature Size and Functionality in Solution-Processed, Porous Hematite Electrodes for Solar Water Splitting. *Nano Lett.* **2010**, *10*, 4155−4160.

(25) Kim, J. H.; Kim, J. H.; Jang, J.-W.; Kim, J. Y.; Choi, S. H.; Magesh, G.; Lee, J.; Lee, J. S. Awakening Solar Water-Splitting Acitivity of $ZnFe_2O_4$ Nanorods by Hybrid Microwave Annealing. *Adv. Energy Mater.* **2015**, *5*, 1401933.

(26) Jang, Y. J.; Jang, J.-W.; Choi, S. H.; Kim, J. Y.; Kim, J. H.; Youn, D. H.; Kim, W. Y.; Han, S.; Lee, J. S. Tree Branch-Shaped Cupric Oxide for Highly Effective Photoelectrochemical Water Reduction. *Nanoscale* **2015**, *7*, 7624−7631.

(27) Youn, D. H.; Jang, J.-W.; Kim, J. Y.; Jang, J. S.; Choi, S. H.; Lee, J. S. Fabrication of Graphene-Based Electrode in Less Than a Minute Through Hybrid Microwave Annealing. *Sci. Rep.* **2014**, *4*, 5492.

(28) Vayssires, L.; Beermann, N.; Lindquist, S.-E.; Hagfeldt, A. Controlled Aqueous Chemical Growth of Oriented Three-Dimensional Crystalline Nanorod Arrays: Application to Iron (III) Oxides. *Chem. Mater.* **2001**, *13*, 233−235.

(29) Vayssieres, L.; Keis, K.; Hagfeldt, A.; Lindquist, S.-E. Three-Dimensional Array of Highly Oriented Crystalline ZnO Microtubes. *Chem. Mater.* **2001**, *13*, 4395−4398.

(30) Cornuz, M.; Grätzel, M.; Sivula, K. Preferential Orientation in Hematite Films for Solar Hydrogen Production via Water Splitting. *Chem. Vap. Deposition* **2010**, *16*, 291−295.

(31) Nakau, T. Electrical Conductivity of α-Fe_2O_3. *J. Phys. Soc. Jpn.* **1960**, *15*, 727−727.

(32) Benjelloun, D.; Bonnet, J.-P.; Doumerc, J.-P.; Launay, J.-C.; Onillon, M.; Hagenmuller, P. Anisotropy of Electrical Properties of Iron Oxide. *Mater. Chem. Phys.* **1984**, *10*, 503−518.

(33) Kim, J. Y.; Jang, J.-W.; Youn, D. H.; Kim, J. Y.; Kim, E. S.; Lee, J. S. Graphene-Carbon Nanotube Composite as an Effective Conducting Scaffold to Enhance the Photoelectrochemical Water Oxidation Activity of a Hematite Film. *RSC Adv.* **2012**, *2*, 9415−9422.

(34) Ueda, K.; Minegishi, T.; Clune, J.; Nakabayashi, M.; Hisatomi, T.; Nishiyama, H.; Katayama, M.; Shibata, N.; Kubota, J.; Yamada, T.; Domen, K. Photoelectrochemical Oxidation of Water Using $BaTaO_2N$ Photoanodes Prepared by Particle Transfer Method. *J. Am. Chem. Soc.* **2015**, *137*, 2227−2230.

(35) Annamalai, A.; Subramanian, A.; Kang, U.; Park, H.; Choi, S. H.; Jang, J. S. Activation of Hematite Photoanodes for Solar Water Splitting: Effect of FTO Deformation. *J. Phys. Chem. C* **2015**, *119*, 3810−3817.

(36) Sarremi-Yarahmadi, S.; Vaidhyanathan, B.; Wijayantha, K.G. U. Microwave-Assisted Low Temperature Fabrication of Nanostructured α-Fe_2O_3 Electrodes for Solar-Driven Hydrogen Generation. *Int. J. Hydrogen Energy* **2010**, *35*, 10155−10165.

(37) Dotan, H.; Sivula, K.; Grätzel, M.; Rothschild, A.; Warren, S. C. Probing the Photoelectrochemical Properties of Hematite (α-Fe_2O_3) Electrodes Using Hydrogen Peroxide as a Hole Scavenger. *Energy Environ. Sci.* **2011**, *4*, 958−964.

(38) Lin, Y.; Xu, Y.; Mayer, M. T.; Simpson, Z. I.; McMahon, G.; Zhou, S.; Wang, D. Growth of p-Type Hematite by Atomic Layer Deposition and Its Utilization for Improved Solar Water Splitting. *J. Am. Chem. Soc.* **2012**, *134*, 5508−5511.

(39) Du, C.; Yang, X.; Mayer, M. T.; Hoyt, H.; Xie, J.; McMahon, G.; Bischoping, G.; Wang, D. Hematite-Based Water Splitting with Low Turn-On Voltages. *Angew. Chem., Int. Ed.* **2013**, *52*, 12692−12695.

(40) Kim, H.-i.; Moon, G.-h.; Monllor-Satoca, D.; Park, Y.; Choi, W. Solar Photoconversion Using Graphene/TiO_2 Composites: Nanographene Shell on TiO_2 Core versus TiO_2 Nanoparticles on Graphene Sheet. *J. Phys. Chem. C* **2012**, *116*, 1535−1543.

(41) Zaban, A.; Greenshtein, M.; Bisquert, J. Determination of the Electron Lifetime in Nanocrystalline Dye Solar Cells by Open-Circuit Voltage Decay Measurements. *ChemPhysChem* **2003**, *4*, 859−864.

(42) Klahr, B.; Gimenez, S.; Fabregat-Santiago, F.; Hamann, T.; Bisquert, J. Water Oxidation at Hematite Photoelectrodes: The Role of Surface States. *J. Am. Chem. Soc.* **2012**, *134*, 4294−4302.

(43) Klahr, B.; Gimenez, S.; Fabregat-Santiago, F.; Bisquert, J.; Hamann, T. W. Photoelectrochemical and Impedance Spectroscopic Investigation of Water Oxidation with "Co-Pi"-Coated Hematite Electrodes. *J. Am. Chem. Soc.* **2012**, *134*, 16693−16700.

(44) Kim, J. Y.; Jun, H.; Hong, S. J.; Kim, H. G.; Lee, J. S. Charge Transfer in Iron Oxide Modified with Carbon Nanotubes for Photoelectrochemical Water Oxidation: An Electrochemical Impedance Study. *Int. J. Hydrogen Energy* **2011**, *36*, 9462−9468.